Dalton Transactions

ROYAL SOCIETY OF CHEMISTRY

PAPER

View Article Online
View Journal | View Issue

Cite this: *Dalton Trans.*, 2025, **54**, 5731

Strong upconverted circularly polarized emission from a chiral tetrahedral Yb/Eu cage†

Zhiwei Yao, Ting Gao, Pengfei Yan, Yanyan Zhou* and Hongfeng Li *

Received 27th January 2025,
Accepted 6th March 2025

DOI: 10.1039/d5dt00219b

rsc.li/dalton

Upconverted circularly polarized luminescence (UC-CPL) materials have attracted significant attention due to their potential in optical sensing and bioimaging. However, achieving UC-CPL in lanthanide supramolecular systems remains a challenge due to the extended distances between lanthanide ions. Here, enantiopure tetrahedral cages, $(Yb/Eu)_4\mathbf{L}_4(R/S\text{-BINAPO})_4$, are assembled using achiral C_3-symmetric ligands, Ln(III) ions and chiral ancillary ligands. Upon 980 nm excitation, the heterometallic tetrahedral cages exhibit strong UC-CPL (g_{lum} = 0.22) and high Φ_{UC} of 3.50×10^{-6}. Moreover, through femtosecond transient absorption spectroscopy, we reveal that the ligand's triplet state (T_1) serves as a critical mediator in the upconversion energy transfer process within the lanthanide complex, facilitating the efficient transfer of energy from the excited state of Yb^{3+} to the Eu^{3+} center *via* the mechanistic pathway Yb** → T_1 → Eu*.

Introduction

Lanthanide complexes with upconverted circularly polarized luminescence (UC-CPL) offer notable advantages over other lanthanide-doped upconversion materials (such as inorganic upconversion nanoparticle materials,[1,2] quantum dots,[3,4] *etc.*), including high biocompatibility, facile solution processing, and structural and functional tunability.[5–7] These attributes make them promising candidates for diverse applications such as cellular imaging,[8,9] remote cellular activation,[10] and photodynamic therapy.[11,12] Except for the two-photon absorption of the chromophore/ligand, the UCL in lanthanide complexes primarily depends on energy transfer between Ln^{3+} ions. To achieve efficient upconversion luminescence, various strategies have been employed to shorten the distance between Ln···Ln ions, including the use of bridging atoms,[13–15] co-crystallization,[16,17] and cluster formation.[18–20]

Auzel has previously suggested that short distances between Ln^{3+} ions (typically less than 5 Å) are crucial for the CLU process.[21] However, in the design of lanthanide supramolecular structures with specific functions, the use of larger-sized ligands often results in an increased distance between lanthanide ions, typically exceeding 5 Å. For example, in the simplest helicate, the distance between lanthanide ions usually ranges from 7 to 15 Å,[22–28] whereas in more complex multinuclear tetrahedral and octahedral structures, the distance between most lanthanide ions is also at least over 8 Å.[29,30] Such longer distances between lanthanide ions can adversely affect the upconversion energy transfer. As a result, finding a new energy transfer mechanism is particularly important. An important advantage of ligand involvement in the upconversion process is its ability to overcome the limitations imposed by Ln···Ln distances, making the preparation of structurally diverse lanthanide supramolecules with upconversion luminescence properties feasible, thereby broadening the potential application scope of upconversion-lanthanide complexes.

β-Diketonate ligands, widely recognized as excellent sensitizers for lanthanide luminescence,[31,32] offer a promising avenue for investigating the role of triplet states in upconversion. Multitopic β-diketone ligands can form polynuclear structures such as helicates,[33–35] tetrahedra,[36] and octahedra.[37] These diverse structures typically endow them with new properties, for instance, supramolecular chirality[38] or host–guest recognition.[39] We anticipate that a well-designed multitopic β-diketonate lanthanide complex will contribute to the study of triplet state involvement in upconversion due to the following advantages: (1) β-diketonate lanthanide complexes typically exhibit 100% intersystem crossing efficiency,[40] which will increase the likelihood of triplet state participation in the upconversion process. (2) The relatively low triplet state energy level (T_1 < 20 000 cm^{-1}) of aryl-containing β-diketones allows for energy transfer from the virtual energy level of Yb^{3+} (490 nm, 20 480 cm^{-1}) generated by two-photon excitation

Key Laboratory of Functional Inorganic Material Chemistry, Ministry of Education, School of Chemistry and Materials Science Heilongjiang University, 74 Xuefu Road, Harbin 150080, China. E-mail: lihongfeng@hlju.edu.cn, zhouyanyan@hlju.edu.cn

†Electronic supplementary information (ESI) available: Synthesis process, characterization, ESI-TOF-MS and ^1H NMR spectra of the complexes. X-ray crystallographic data for $(Yb_4L_4)(R\text{-BINAPO})_4$. CCDC 2416911. For ESI and crystallographic data in CIF or other electronic format see DOI: https://doi.org/10.1039/d5dt00219b

(980 nm) to the T_1 state.[41] (3) The design of multitopic β-diketonates with long spacers can extend the distance between Ln^{3+} ions, thereby minimizing interference from Ln → Ln energy transfer and clarifying the participation of the T_1 state.

Based on these considerations, we designed and synthesized the chiral lanthanide heteropolynuclear tetrahedral cages $Ln_4\mathbf{L}_4$(*R*/*S*-BINAPO)$_4$ with upconverted circularly polarized luminescence properties. Upon excitation at 980 nm, the chiral tetrahedral cages (Yb/Eu)$_4\mathbf{L}_4$(*R*/*S*-BINAPO)$_4$ show excellent upconverted circularly polarized luminescence, with a maximum $|g_{lum}|$ value of 0.22 at 595 nm. This obvious UC-CPL performance is driven by an upconversion energy transfer process mediated by the ligand triplet state (T_1), promoting the potential of supramolecular cages in advanced luminescence applications (Scheme 1).

Results and discussion

Synthesis and characterization of the tetrahedral cages

The preparation of the ligand **L** was conducted according to literature procedures.[30] The tetrahedral cage $Yb_4\mathbf{L}_4$(*R*-BINAPO)$_4$ was prepared by the self-assembly of the ligand and *R*-BINAPO with $YbCl_3{\cdot}6H_2O$ salts in a 1 : 1 : 1 ratio in CH_3OH at room temperature. Owing to the low resolution of the ^{1}H NMR spectra for $Yb_4\mathbf{L}_4$(*R*-BINAPO)$_4$ (Fig. S1†), the isostructural Lu(III) complex $Lu_4\mathbf{L}_4$(*R*-BINAPO)$_4$ was used as a surrogate for NMR analyses (Fig. S4 and S5;† ^{1}H–^{1}H COSY and ^{1}H–^{1}H NOESY). As illustrated in Fig. 1b, the $Lu_4\mathbf{L}_4$(*R*-BINAPO)$_4$ complex exhibits a single set of broadened but distinguishable proton resonances. Compared to the free ligand **L** and the ancillary ligand *R*-BINAPO, the majority of the signals from the tetrahedral cage experience significant upfield shifts. The three distinct resonances corresponding to the tris(β-diketone) moiety exhibit broadening and relatively large shifts upon coordination with the metal center. Furthermore, no additional peaks associated with **L** were observed, suggesting the high diastereopurity of the self-assembled cages. The ^{31}P and ^{19}F NMR spectra further confirm the formation of a single species, as evidenced by the presence of a single, sharp singlet peak for the cage complex $Lu_4\mathbf{L}_4$(*R*-BINAPO)$_4$ (Fig. S6 and S7†). In ^{1}H diffusion-ordered NMR spectroscopy (DOSY), the cage $Lu_4\mathbf{L}_4$(*R*-BINAPO)$_4$ displays one diffusion band at a diffusion coefficient of $D = 4.16 \times 10^{-10}$ m^2 s^{-1} in line with the formation of a single species with a hydrodynamic diameter of 19 Å, estimated by the Stokes–Einstein equation (Fig. 1c). The dynamic diameter of the complex is in good agreement with that observed from the crystal structure of $Yb_4\mathbf{L}_4$(*R*-BINAPO)$_4$. The formation of $Yb_4\mathbf{L}_4$(*R*-BINAPO)$_4$ in solution was further confirmed by high-resolution electrospray ionization mass spectrometry (ESI-TOF-MS) (Fig. S8†). The spectrum exhibits molecular ions corresponding to the formula $Yb_4\mathbf{L}_4$(BINAPO)$_4$, and the observed isotopic distribution aligns with the theoretical profile for the $[Yb_4\mathbf{L}_4(BINAPO)_4 + H]^+$ species.

To further determine the chemical structure and composition of tetrahedral $Yb_4\mathbf{L}_4$(*R*-BINAPO)$_4$, yellow square-shaped crystals were obtained by slow diffusion of hexane into its tetrahydrofuran solution at room temperature. X-ray diffraction analysis confirms that the complex $Yb_4\mathbf{L}_4$(*R*-BINAPO)$_4$ adopts the anticipated M_4L_4 tetrahedral architecture (Fig. 2d) and crystallizes in the chiral space group C_2. This observation indicates that chirality from the *R*-BINAPO ligand is successfully transferred into the tetrahedral architecture. Within the cage, four Yb(III) ions are positioned at the vertices, while four ligands occupy the four faces. Each Yb center is coordinated by three β-diketonate moieties of the three ligands and one BINAPO ancillary ligand, forming a distorted triangular dodecahedral coordination geometry (Fig. S19†). In $Yb_4\mathbf{L}_4$(*R*-BINAPO)$_4$, the β-diketonate units helically twist each Yb(III) center in a left-handed, propeller-like manner, establishing a Λ configuration at each of the four vertices.

To investigate the upconversion luminescence properties of the heteropolynuclear tetrahedral cages ($Yb_xEu_{4-x}\mathbf{L}_4$)(*R*/*S*-BINAPO)$_4$ (x = 0.5–3.5) in solution, the ($Yb_xEu_{4-x}\mathbf{L}_4$)(*R*/*S*-BINAPO)$_4$ assemblies with different molar ratios of Yb^{3+} and Eu^{3+} ions were also synthesized by a similar synthesis method to that for ($Yb_4\mathbf{L}_4$)(*R*-BINAPO)$_4$. The heteropolynuclear tetrahedral cages ($Yb_xEu_{4-x}\mathbf{L}_4$)(*R*-BINAPO)$_4$ were characterized *via* ESI-TOF-MS and NMR spectra (Fig. S9–S18†).

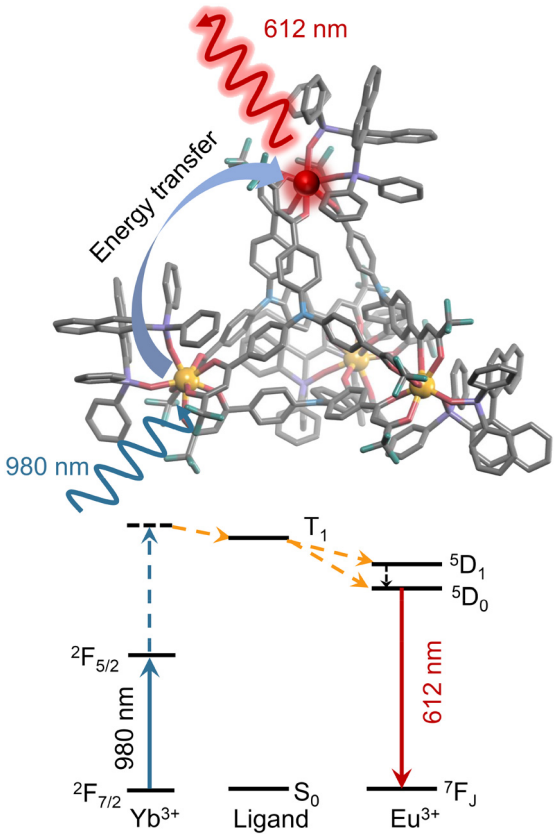

Scheme 1 Schematic of upconversion luminescence of Eu^{3+} upon excitation of the Yb^{3+} ion (λ_{ex} = 980 nm) (upper) and energy transfer mechanism (lower) in (Yb/Eu)$_4$L$_4$(*R*/*S*-BINAPO)$_4$ with upconversion luminescence.

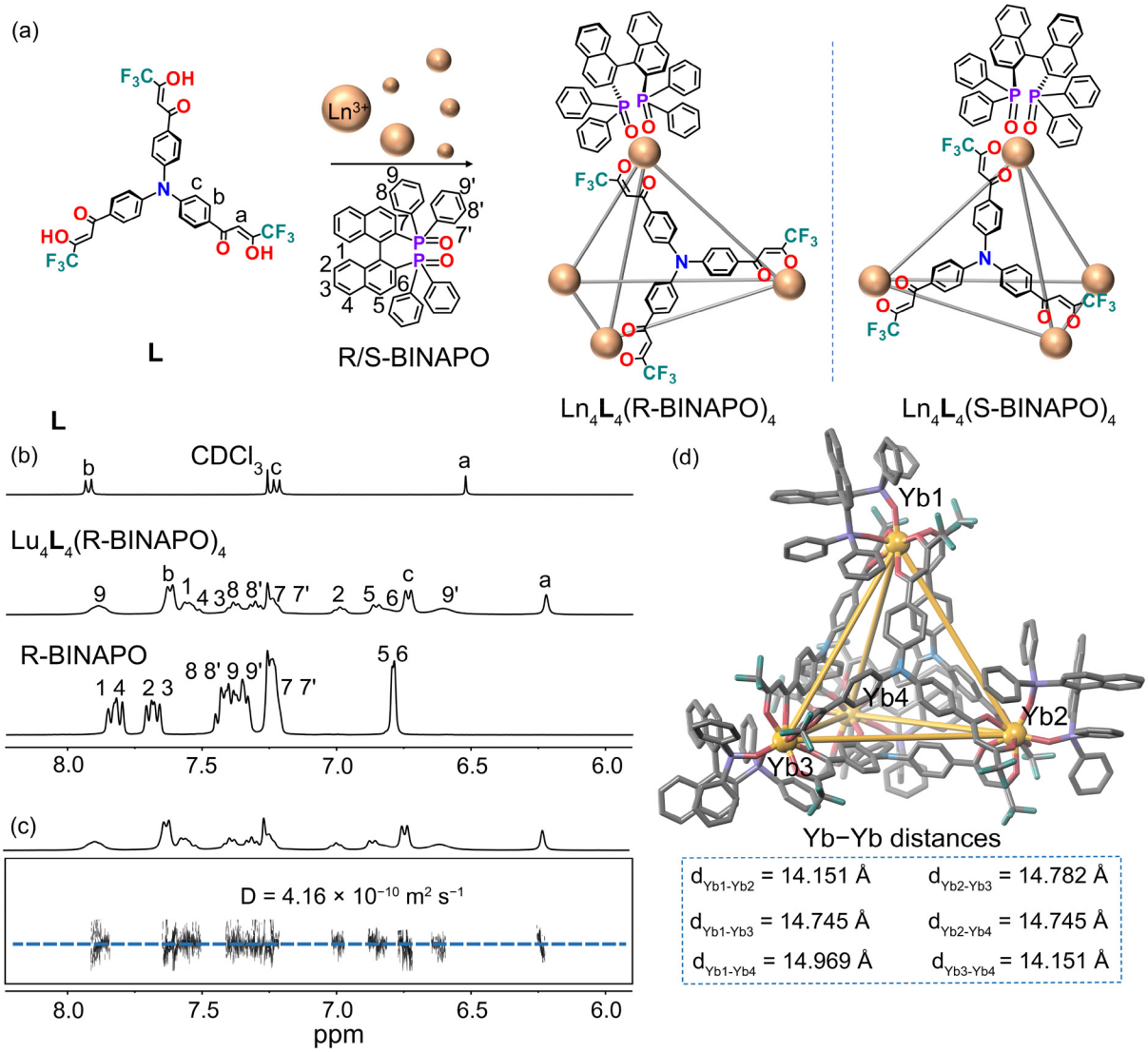

Fig. 1 (a) Self-assembly of Ln_4L_4(*R*/*S*-BINAPO)$_4$ cages. (b) ^{1}H NMR spectra (400 MHz, 298 K) of free ligand **L**, (*R*)-BINAPO, and Lu_4L_4(*R*-BINAPO)$_4$ in $CDCl_3$. (c) ^{1}H DOSY spectrum (400 MHz, 298 K) of Lu_4L_4(*R*-BINAPO)$_4$ in $CDCl_3$. (d) Crystallographic structure of Yb_4L_4(*R*-BINAPO)$_4$.

Upconversion emission behavior of heterometallic tetrahedral cages ($Yb_xEu_{4-x}L_4$)(*R*/*S*-BINAPO)$_4$

As shown in Fig. 2a, the upconversion luminescence properties of the tetrahedral cages were studied under 980 nm excitation at room temperature in $CHCl_3$. The emission spectra of ($Yb_xEu_{4-x}L_4$)(*R*-BINAPO)$_4$ (x = 0.5–3.5) all show five characteristic emission bands at 580, 594, 612, 650, and 702 nm, respectively, related to the $^5D_0 \rightarrow {}^7F_J$ (J = 0–4) transitions. Among the seven assemblies of ($Yb_xEu_{4-x}L_4$)(*R*-BINAPO)$_4$ (x = 0.5–3.5), the assembly of ($Yb_{2.5}Eu_{1.5}L_4$)(*R*-BINAPO)$_4$ exhibits the most intense upconversion luminescence. The higher molar ratio of Yb^{3+} ions in ($Yb_xEu_{4-x}L_4$)(*R*-BINAPO)$_4$ may increase the energy transfer between Yb^{3+} ions, leading to a decrease in the energy transfer from Yb^{3+} to Eu^{3+},[42,43] while a lower molar ratio of the sensitizer Yb^{3+} is usually insufficient to activate the Eu^{3+} ions.[44,45]

To further investigate the upconversion luminescence process of the heteropolynuclear tetrahedral cages ($Yb_xEu_{4-x}L_4$)(*R*-BINAPO)$_4$ (x = 0.5–3.5), the corresponding upconversion emission intensities of the tetrahedral cages were integrated as a function of 980 nm laser power density (P = 2.0–37.4 W cm^{-2}) (Fig. 2b and S21–S24†). The slopes of logarithm I (I = integrated areas of luminescence intensity) *versus* logarithm P (laser power density, W cm^{-2}) are related to the photon number to sensitize the $^5D_0$ excited state of Eu^{3+}.[46] The slope values of ($Yb_xEu_{4-x}L_4$)(*R*/*S*-BINAPO)$_4$ (x = 0.5–3.5) are all around 2.0 in $CHCl_3$, strongly suggesting two-photon absorption characteristics of Eu^{3+} ion emission (Fig. 2d and S25–S28†). In addition, after being stored in a desiccator for 3 months, the upconversion emission intensity of ($Yb_{2.5}Eu_{1.5}L_4$)(*R*-BINAPO)$_4$ exhibits only a slight decrease (Fig. S29 and S30†), indicating its high structural stability and upconversion luminescence performance.

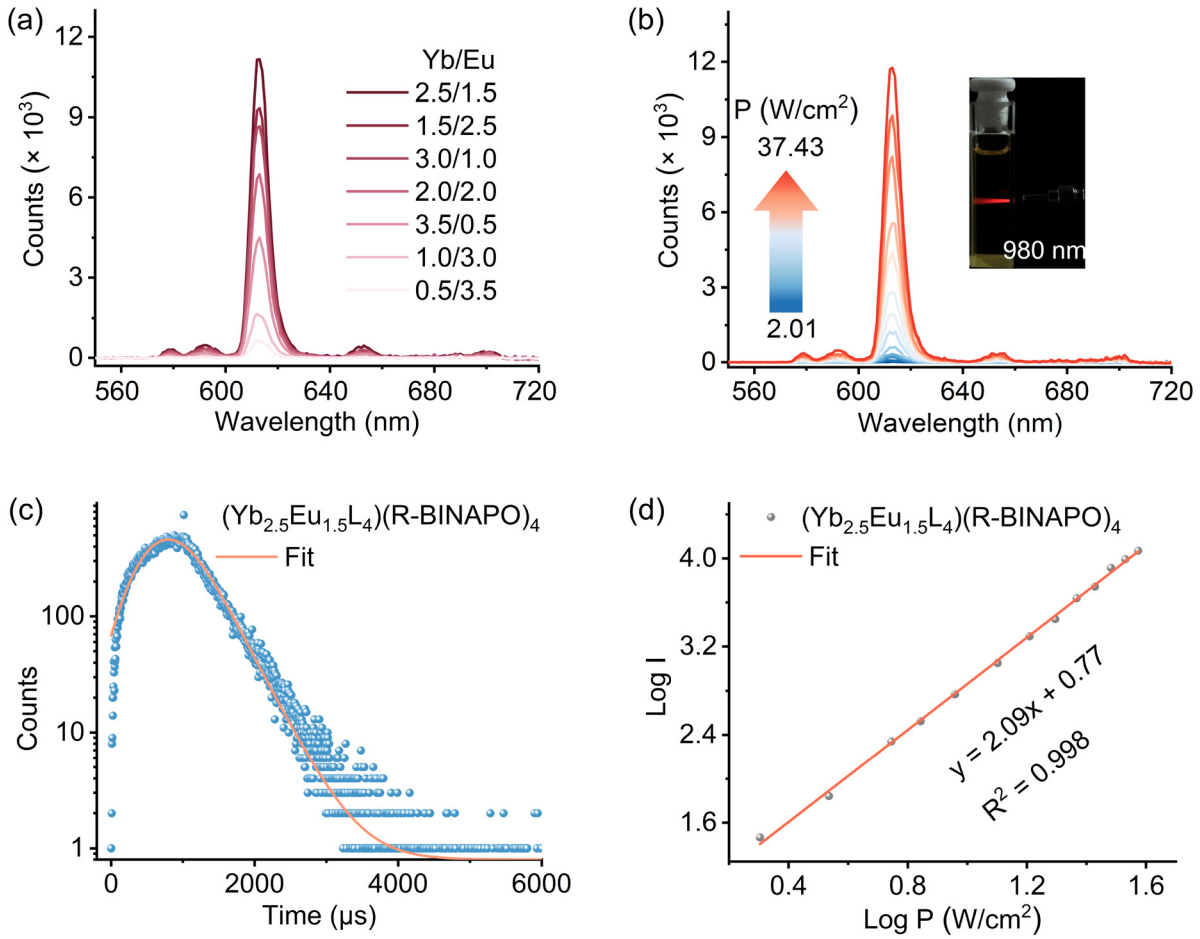

Fig. 2 (a) Upconversion luminescence spectra of $(Yb_xEu_{4-x}L_4)(R\text{-BINAPO})_4$ (x = 0.5–3.5) assemblies in $CHCl_3$, λ_{ex} = 980 nm. (b) Upconversion emission spectra of $(Yb_{2.5}Eu_{1.5}L_4)(R\text{-BINAPO})_4$ in $CHCl_3$ with variable laser power (λ_{ex} = 980 nm) focused on a spot size of ~0.13 cm^2. (c) Time-resolved decay of the UC emission at 612 nm of $(Yb_{2.5}Eu_{1.5}L_4)(R\text{-BINAPO})_4$ in $CHCl_3$. (d) The corresponding log–log plots of the UC intensity integrated (I) from 570 to 720 nm of $(Yb_{2.5}Eu_{1.5}L_4)(R\text{-BINAPO})_4$ as a function of the laser power density P (in W cm^{-2}).

Then, the luminescence lifetime of $(Yb_{2.5}Eu_{1.5}L_4)(R\text{-BINAPO})_4$ was studied upon 980 nm excitation (Fig. 2c). The decay time of the upconversion signal at 612 nm for $(Yb_{2.5}Eu_{1.5}L_4)(R\text{-BINAPO})_4$ in $CHCl_3$ was determined by fitting the decay curves to a single exponential function, which is consistent with the observations under 395 nm excitation (Fig. S31†). Therefore, this suggests that only a single species is present in the excited state of the complex. Using $[(YbL)_2Tb_1]$ (Φ_{ref} = 1.4 × 10^{-8}) as the reference,[16] the upconversion luminescence quantum yield (Φ_{UC}) of the cage $(Yb_{2.5}Eu_{1.5}L_4)(R\text{-BINAPO})_4$ was estimated to be 3.50 × 10^{-6} (P = 37.43 W cm^{-2}, Fig. S37–40†). We propose that the relatively high upconversion luminescence quantum yield of the heteropolynuclear tetrahedral cage mainly arises from the incorporation of PO ancillary ligands, which not only enhances the rigidity of the tetrahedral skeleton but also prevents solvent molecules from entering the coordination sphere of the metal ions, thus inhibiting nonradiative transition.

The chiroptical activity of $(Yb_{2.5}Eu_{1.5}L_4)(R/S\text{-BINAPO})_4$ in $CHCl_3$ was verified by circular dichroism (CD) spectroscopy (Fig. 3b left). The enantiomeric cages display mirror-image CD

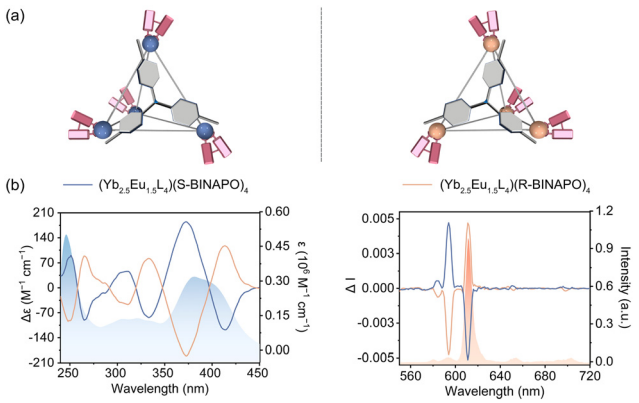

Fig. 3 (a) Schematic illustration of the enantiopure tetrahedral cages $(Yb_{2.5}Eu_{1.5}L_4)(R/S\text{-BINAPO})_4$. (b) Left: UV-visible absorption and CD spectra of $(Yb_{2.5}Eu_{1.5}L_4)(R/S\text{-BINAPO})_4$ in $CHCl_3$ (2.5 × 10^{-6} M). Right: total luminescence and upconverted CPL spectra of $(Yb_{2.5}Eu_{1.5}L_4)(R/S\text{-BINAPO})_4$ in $CHCl_3$ (λ_{ex} = 980 nm, 2.5 × 10^{-3} M).

signals in the range of 250–500 nm, with a negative exciton couplet for the Λ-configurational $(Yb_{2.5}Eu_{1.5}\mathbf{L}_4)(R\text{-BINAPO})_4$ and a perfect mirror-image for the Δ-configurational $(Yb_{2.5}Eu_{1.5}\mathbf{L}_4)(S\text{-BINAPO})_4$. This correlation between the Δ/Λ configuration and the exciton couplet sign aligns with the empirical rule.[47] The band in the 240–292 nm region is attributed to the π–π* transition of the chiral BINAPO. However, two distinct Cotton effects were observed within the absorption range (292–450 nm) of the achiral tris-β-diketone ligands. This result suggests that the chirality of *R*/*S*-BINAPO was effectively transferred to the achiral tris-β-diketone ligand, resulting in the formation of helical chirality in the tetrahedral cage.

Benefiting from the homochirality of the multimetallic tetrahedral cages $(Yb_{2.5}Eu_{1.5}\mathbf{L}_4)(R/S\text{-BINAPO})_4$, we explored their upconverted CPL properties. As expected, $(Yb_{2.5}Eu_{1.5}\mathbf{L}_4)(R/S\text{-BINAPO})_4$ exhibit upconverted CPL properties upon 980 nm excitation in $CHCl_3$ (Fig. 3b right). A pair of heteropolynuclear tetrahedron cages show mirror-image CPL spectra; the two opposite major signals at 595 nm and 612 nm correspond to the transitions of $^5D_0 \rightarrow {}^7F_1$ ($\Delta J = 1$) and $^5D_0 \rightarrow {}^7F_2$ ($\Delta J = 2$), respectively. Despite the lower emission intensity of the $^5D_0 \rightarrow {}^7F_1$ transition, its unique magnetic-dipole character results in a higher degree of circularly polarized emission compared to the $^5D_0 \rightarrow {}^7F_2$ transition. The luminescence asymmetry factor (g_{lum}) is a key parameter for quantifying the magnitude of upconverted circularly polarized luminescence (UC-CPL). It is defined as $g_{lum} = 2(I_L - I_R)/(I_L + I_R)$, where I_L and I_R represent the left- and right-polarized emission intensities, respectively, with the condition that $-2 \leq g_{lum} \leq 2$. Notably, the tetrahedral cages $(Yb_{2.5}Eu_{1.5}\mathbf{L}_4)(R/S\text{-BINAPO})_4$ exhibit a luminescence dissymmetry factor (g_{lum}) of up to 0.22 at the Eu^{3+} center under 980 nm excitation. Moreover, the heteropolynuclear tetrahedral cages $(Yb_xEu_{4-x}\mathbf{L}_4)(R/S\text{-BINAPO})_4$ with other compositions also show favorable upconverted CPL properties, and their g_{lum} values are summarized in Table S2.†

Upconversion luminescence mechanism discussion

To date, four principal mechanisms underlying energy upconversion luminescence have been delineated: excited-state absorption (ESA),[48] energy transfer (ETU),[49,50] cooperative luminescence (CLU),[51] and cooperative sensitized upconversion (CSU),[52] despite the relatively limited research on upconversion luminescence in lanthanide complexes. Recently, Sun discovered a novel mechanism in which excited multimers participate in the upconversion cooperative sensitization process.[53] Firstly, the emission spectrum of the homonuclear complex $(Eu_4\mathbf{L}_4)(R\text{-BINAPO})_4$ was measured under 980 nm excitation, but no upconversion emission was observed, which rules out the pathway involving ligand two-photon absorption sensitization (Fig. S32†). Therefore, the two-photon UC luminescence from $(Yb/Eu)_4\mathbf{L}_4(R\text{-BINAPO})_4$ most likely arises from the cooperative luminescence (CLU) or cooperative sensitization (CSU) of two excited Yb^{3+} ions. However, upon excitation of the homonuclear $(Yb_4\mathbf{L}_4)(R\text{-BINAPO})_4$ at 980 nm, neither Yb two-photon upconversion luminescence (490 nm) nor ligand emission is detected in the visible spectral region (Fig. S33†). This result prompted us to speculate that the upconversion luminescence of $(Yb/Eu)_4\mathbf{L}_4(R\text{-BINAPO})_4$ may arise from a bimetallic cooperative mechanism. Azel emphasized that a spatial distance of less than 5 Å between Ln^{3+} ions is crucial for the upconversion luminescence process.[21] According to the crystal structure of the tetrahedral $(Yb_4\mathbf{L}_4)(R\text{-BINAPO})_4$, the Ln⋯Ln distances range from 14.15 to 14.97 Å (Fig. 1d), suggesting that cooperative interactions between Yb*/Yb* should be difficult to realize. Additionally, the UC emission observed for the tetrahedral cage in solution rules out the possibility of a cooperative mechanism due to reduced Yb⋯Yb distances in the aggregated state. Therefore, considering the Ln⋯Ln distance and the absence of upconversion emission from Yb*/Yb* or the ligands in the visible spectral region, we hypothesize the presence of another energy transfer mechanism involving continuous absorption through Yb two-photon absorption (ESA), followed by energy transfer from the ligand's triplet state to the Eu^{3+} ion.

To investigate the possible participation of the ligand triplet states (T_1) in the upconversion (UC) process, we first determined the triplet energy level of the auxiliary ligand to be 26 666 cm^{-1} through phosphorescence spectroscopy (Fig. S34†). This value significantly exceeds the virtual state energy level of Yb^{3+} in two-photon absorption (20 408 cm^{-1}, 490 nm), thereby ruling out the possibility of the auxiliary ligand participating in the upconversion process. Based on our previous work,[54] the triplet energy level of ligand **L** is 19 194 cm^{-1}, indicating that ligand **L** fulfills the necessary conditions to participate in the upconversion process. However, under 980 nm excitation at 77 K, no emission associated with short- or long-lifetime fluorescence or phosphorescence was detected in the visible spectral region for $(Yb_{2.5}Gd_{1.5}\mathbf{L}_4)(R\text{-BINAPO})_4$ (Fig. S35†). This indicates that either the triplet states (T_1) are not present or rapid energy transfer from the T_1 state to the $^2F_{5/2}$ state of Yb^{3+} ions occurs, leading to the quenching of ligand phosphorescence. Femtosecond transient absorption spectroscopy (fs-TAS) was then employed on $(Yb_4\mathbf{L}_4)(R\text{-BINAPO})_4$ to investigate this ultrafast dynamic process. Under 980 nm femtosecond pulse excitation, a transient absorption band corresponding to the triplet state (T_1) of the ligand was clearly observed in the 470–700 nm range (Fig. 4). This result unequivocally confirms the occurrence of an energy transfer process from Yb** to the ligand triplet state. Moreover, the lifetime of T_1 was estimated to be 0.494 ps by fitting the kinetic curve of the TAS absorption (Fig. 4d). This value is notably shorter than the 2.7 ms lifetime of the ligand triplet state observed in $(Gd_4\mathbf{L}_4)(R\text{-BINAPO})_4$ (Fig. S36†), suggesting an efficient and rapid energy transfer from the T_1 state to the $^2F_{5/2}$ state in the Eu/Yb heterometallic assembly. Furthermore, the rapid energy transfer rate from the T_1 state to Eu(III) can be derived using eqn (1):

$$k_{ET} = \frac{1}{\tau} - \frac{1}{\tau_0} \quad (1)$$

where τ represents the excited-state lifetime in the presence of energy transfer, and τ_0 denotes the intrinsic excited-state life-

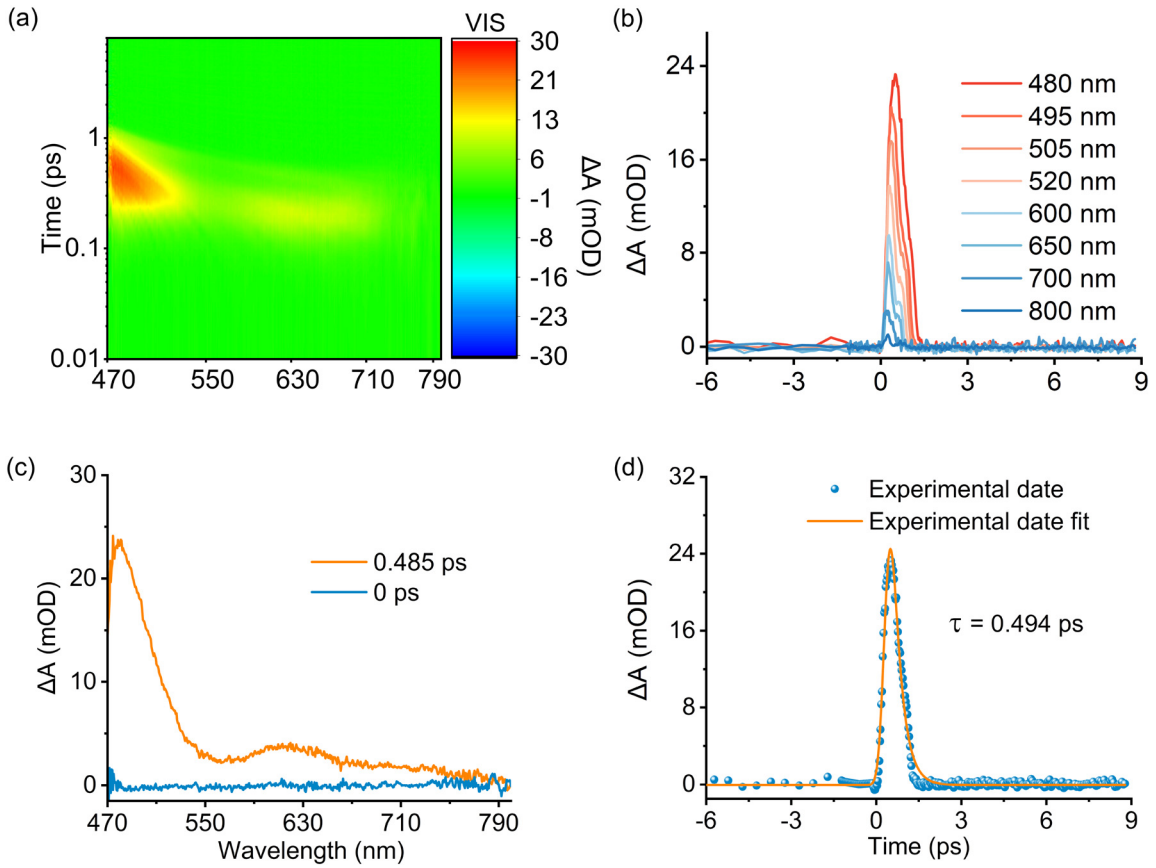

Fig. 4 (a) 2D fs-TAS spectrum of Yb_4L_4(*R*-BINAPO)$_4$ represented as a color map in $CHCl_3$ (2.5×10^{-3} M, λ_{ex} = 980 nm). (b) Normalized decays of fs transient absorption at selected wavelengths. (c) Fs transient absorption spectra of Yb_4L_4(*R*-BINAPO)$_4$. (d) A comparison of the exponential fitting results for the observed TAS data at 480 nm probe wavelength.

time in the absence of energy transfer. Based on this equation, the calculated k_{ET} value is 2.02×10^{12} s^{-1}. Overall, these results provide strong evidence for an energy transfer process involving triplet states in lanthanide upconversion luminescence (UCL), where energy is transferred from Yb** *via* the ligand triplet state (T_1) to the Eu^{3+} ion (Yb** → T_1 → Eu*). Meanwhile, during the preparation of this manuscript, the Sun group also discovered this upconversion luminescence mechanism.[55]

Conclusion

In summary, under 980 nm excitation, the chiral heterometallic tetrahedral cages ($Yb_{2.5}Eu_{1.5}$**L**$_4$)(*R*/*S*-BINAPO)$_4$ exhibit strong upconverted circularly polarized luminescence (UC-CPL) properties ($|g_{lum}|$ = 0.22) and a high upconversion luminescence quantum yield of 3.50×10^{-6}. This excellent UC-CPL performance is attributed to the rigid and saturated chiral environment created by the ancillary ligand *R*/*S*-BINAPO and the effective participation of the ligand triplet state in the upconversion luminescence process, where energy is transferred from Yb** through the triplet state (T_1) of the ligand to the Eu^{3+} ion (Yb** → T_1 → Eu*). This work expands the application of lanthanide supramolecules in the UC-CPL field.

Author contributions

H. F. L. conceived and supervised the project. Z. W. Y. performed the experiments and analysed the data. Y. Y. Z. collected diffraction data and solved and refined the X-ray crystal structures. H. F. L., Y. Y. Z., T. G. and P. F. Y. reviewed and edited the paper. All authors contributed to the final draft of the paper.

Data availability

The data that support the findings of this study, including X-ray crystallographic data for (Yb_4L_4)(*R*-BINAPO)$_4$, are available in the ESI† of this article. Crystallographic data have been deposited at the Cambridge Crystallographic Data Centre as entry CCDC 2416911.†

Conflicts of interest

The authors declare no conflict of interest.

Acknowledgements

This work was financially supported by the National Natural Science Foundation of China (No. 52273263, and 52203219) and the Scientific Research Project of Basic Scientific Research Operating Expenses of Colleges and Universities in Heilongjiang Province (2021-KYYWF-0029 and 2021-KYYWF-0041).

References

1 H. Zhang, H. Wei, L. Xu, Y. Li, Z. Song, D. Zhou, Q. Wang, Z. Long, Y. Yang, Y. Wen, J. Han, Y. Gao and J. Qiu, *Ceram. Int.*, 2023, **49**, 30436–30442.
2 H. He, M. Cen, J. Wang, Y. Xu, J. Liu, W. Cai, D. Kong, K. Li, D. Luo, T. Cao and Y. J. Liu, *ACS Appl. Mater. Interfaces*, 2022, **14**, 53981–53989.
3 J. Zhao and P. Xing, *ChemPhotoChem*, 2021, **6**, e202100124.
4 B. Tang, Q. Wei, S. Wang, H. Liu, N. Mou, Q. Liu, Y. Wu, A. S. Portniagin, S. V. Kershaw, X. Gao, M. Li and A. L. Rogach, *Small*, 2024, **20**, 2311639.
5 E. G. Percástegui, T. K. Ronson and J. R. Nitschke, *Chem. Rev.*, 2020, **120**, 13480–13544.
6 E. G. Percástegui, *Eur. J. Inorg. Chem.*, 2021, **2021**, 4425–4438.
7 X.-Z. Li, C.-B. Tian and Q.-F. Sun, *Chem. Rev.*, 2022, **122**, 6374–6458.
8 W. Ralph and N. Vasilis, *Nat. Med.*, 2003, **9**, 123–128.
9 Y. Kargar Gaz Kooh and N. Huebsch, *Front. Mech. Eng.*, 2024, **10**, 1481933.
10 X. Ai, L. Lyu, Y. Zhang, Y. Tang, J. Mu, F. Liu, Y. Zhou, Z. Zuo, G. Liu and B. Xing, *Angew. Chem., Int. Ed.*, 2017, **56**, 3031–3035.
11 X. Zhang, F. Ai, T. Sun, F. Wang and G. Zhu, *Inorg. Chem.*, 2016, **55**, 3872–3880.
12 G. Xu, C. Li, C. Chi, L. Wu, Y. Sun, J. Zhao, X.-H. Xia and S. Gou, *Nat. Commun.*, 2022, **13**, 3064.
13 A. Nonat, C. F. Chan, T. Liu, C. Platas-Iglesias, Z. Liu, W.-T. Wong, W.-K. Wong, K.-L. Wong and L. J. Charbonnière, *Nat. Commun.*, 2016, **7**, 11978.
14 L. Aboshyan-Sorgho, C. Besnard, P. Pattison, K. R. Kittilstved, A. Aebischer, J. C. G. Bünzli, A. Hauser and C. Piguet, *Angew. Chem., Int. Ed.*, 2011, **50**, 4108–4112.
15 J. Wang, Y. Jiang, J. Y. Liu, H. B. Xu, Y. X. Zhang, X. Peng, M. Kurmoo, S. W. Ng and M. H. Zeng, *Angew. Chem., Int. Ed.*, 2021, **60**, 22368–22375.
16 A. Nonat, S. Bahamyirou, A. Lecointre, F. Przybilla, Y. Mély, C. Platas-Iglesias, F. Camerel, O. Jeannin and L. J. Charbonnière, *J. Am. Chem. Soc.*, 2019, **141**, 1568–1576.
17 G. Sun, Y. Xie, Y. Wang, G. A. Mandl, S. L. Maurizio, H. Zhang, X. Ottenwaelder, J. A. Capobianco and L. Sun, *Angew. Chem., Int. Ed.*, 2023, **62**, e202304591.
18 D. A. Gálico, J. S. Ovens, F. A. Sigoli and M. Murugesu, *ACS Nano*, 2021, **15**, 5580–5585.
19 R. C. Knighton, L. K. Soro, A. Lecointre, G. Pilet, A. Fateeva, L. Pontille, L. Francés-Soriano, N. Hildebrandt and L. J. Charbonnière, *Chem. Commun.*, 2021, **57**, 53–56.
20 S. P. K. Panguluri, E. Jourdain, P. Chakraborty, S. Klyatskaya, M. M. Kappes, A. M. Nonat, L. J. Charbonnière and M. Ruben, *J. Am. Chem. Soc.*, 2024, **146**, 13083–13092.
21 F. Auzel and P. Goldner, *Opt. Mater.*, 2001, **16**, 93–103.
22 K.-H. Yim, C.-T. Yeung, H.-Y. Wong and G.-L. Law, *Inorg. Chem. Front.*, 2021, **8**, 2952–2964.
23 J. K. Clegg, F. Li and L. F. Lindoy, *Coord. Chem. Rev.*, 2022, **455**, 214355.
24 C.-T. Yeung, W. T. K. Chan, S.-C. Yan, K.-L. Yu, K.-H. Yim, W.-T. Wong and G.-L. Law, *Chem. Commun.*, 2015, **51**, 592–595.
25 R. Diego, M. Darawsheh, L. A. Barrios, A. Sadurní, J. García, P. Lloyd-Williams, S. J. Teat, O. Roubeau, D. Aguilà and G. Aromí, *Dalton Trans.*, 2019, **48**, 16844–16847.
26 X. Gao, L. Li, W. Sun and P. Chen, *Dalton Trans.*, 2020, **49**, 2843–2849.
27 R. Chen, Q.-Q. Yan, S.-J. Hu, X.-Q. Guo, L.-X. Cai, D.-N. Yan, L.-P. Zhou and Q.-F. Sun, *Org. Chem. Front.*, 2021, **8**, 2576–2582.
28 X. Wang, Q. Ma, S. Yin, T. Gao, P. Yan, Y. Zhou and H. Li, *Dalton Trans.*, 2025, **54**, 1343–1347.
29 C.-T. Yeung, K.-H. Yim, H.-Y. Wong, R. Pal, W.-S. Lo, S.-C. Yan, M. Yee-Man Wong, D. Yufit, D. E. Smiles, L. J. McCormick, S. J. Teat, D. K. Shuh, W.-T. Wong and G.-L. Law, *Nat. Commun.*, 2017, **8**, 1128.
30 Y. Zhou, H. Li, T. Zhu, T. Gao and P. Yan, *J. Am. Chem. Soc.*, 2019, **141**, 19634–19643.
31 I. F. Costa, L. Blois, T. B. Paolini, I. P. Assunção, E. E. S. Teotonio, M. C. F. C. Felinto, R. T. Moura, Jr., R. L. Longo, W. M. Faustino, L. D. Carlos, O. L. Malta, A. N. C. Neto and H. F. Brito, *Coord. Chem. Rev.*, 2024, **502**, 215590.
32 V. I. Vovna, V. V. Korochentsev, A. I. Cherednichenko and A. V. Shurygin, *Russ. Chem. Bull.*, 2015, **8**, 1701–1712.
33 Y. B. Tan, Y. Okayasu, S. Katao, Y. Nishikawa, F. Asanoma, M. Yamada, J. Yuasa and T. Kawai, *J. Am. Chem. Soc.*, 2020, **142**, 17653–17661.
34 Y. Zhang, Y. Zhou, T. Gao, P. Yan and H. Li, *Chem. Commun.*, 2020, **56**, 13213–13216.
35 Y. Zhou, Y. Yao, Z. Cheng, T. Gao, H. Li and P. Yan, *Inorg. Chem.*, 2020, **59**, 12850–12857.
36 W. Li, Y. Zhou, T. Gao, J. Li, S. Yin, W. Huang, Y. Li, Q. Ma, Z. Yao, P. Yan and H. Li, *ACS Appl. Mater. Interfaces*, 2022, **14**, 55979–55988.
37 T. Zhao, Y. F. Zhang, G. H. Wang, X. X. Wang, P. F. Feng and S. Q. Zang, *Angew. Chem., Int. Ed.*, 2025, e202421426.
38 Q. Ma, S. Yin, Z. Song, T. Gao, P. Yan, Y. Zhou and H. Li, *Inorg. Chem. Front.*, 2024, **11**, 8093–8100.

39 Y. Yao, Y. Zhou, T. Zhu, T. Gao, H. Li and P. Yan, *ACS Appl. Mater. Interfaces*, 2020, **12**, 15338–15347.
40 S. Miyazaki, M. Gotanda, Y. Kitagawa, Y. Hasegawa, K. Miyata and K. Onda, *J. Phys. Chem. Lett.*, 2024, **15**, 10718–10724.
41 F. J. Steemers, W. Verboom, D. N. Reinhoudt, E. B. van der Tol and J. W. Verhoeven, *J. Am. Chem. Soc.*, 1995, **117**, 9408–9414.
42 B. Chen and F. Wang, *Acc. Chem. Res.*, 2019, **53**, 358–367.
43 S. Wen, D. Li, Y. Liu, C. Chen, F. Wang, J. Zhou, G. Bao, L. Zhang and D. Jin, *J. Phys. Chem. Lett.*, 2022, **13**, 5316–5323.
44 C. Ma, X. Xu, F. Wang, Z. Zhou, D. Liu, J. Zhao, M. Guan, C. I. Lang and D. Jin, *Nano Lett.*, 2017, **17**, 2858–2864.
45 Y. Wang, G. Sun, Q. Su, Y. Xie, F. Xing, H. Zhang and L. Sun, *Chem. – Eur. J.*, 2024, **30**, e202400911.
46 B. Golesorkhi, A. Fürstenberg, H. Nozary and C. Piguet, *Chem. Sci.*, 2019, **10**, 6876–6885.
47 G. Muller, in *Luminescence oflanthanide ions in coordination compounds and nanomaterials*, ed. A. de Bettencourt-Dias, Wiley, Hoboken, NJ, 2014, pp. 77–124.
48 B. Golesorkhi, A. Fürstenberg, H. Nozary and C. Piguet, *Chem. Sci.*, 2019, **10**, 6876–6885.
49 I. Hyppänen, S. Lahtinen, T. Ääritalo, J. Mäkelä, J. Kankare and T. Soukka, *ACS Photonics*, 2014, **1**, 394–397.
50 D. A. Gálico, J. S. Ovens, F. A. Sigoli and M. Murugesu, *ACS Nano*, 2021, **15**, 5580–5585.
51 L. K. Soro, R. C. Knighton, F. Avecilla, W. Thor, F. Przybilla, O. Jeannin, D. Esteban-Gomez, C. Platas-Iglesias and L. J. Charbonnière, *Adv. Opt. Mater.*, 2022, **11**, 2202307.
52 R. C. Knighton, L. K. Soro, L. Francés-Soriano, A. Rodríguez-Rodríguez, G. Pilet, M. Lenertz, C. Platas-Iglesias, N. Hildebrandt and L. J. Charbonnière, *Angew. Chem., Int. Ed.*, 2021, **61**, e202113114.
53 X.-F. Duan, L.-P. Zhou, H.-R. Li, S.-J. Hu, W. Zheng, X. Xu, R. Zhang, X. Chen, X.-Q. Guo and Q.-F. Sun, *J. Am. Chem. Soc.*, 2023, **145**, 23121–23130.
54 Y. Yao, Y. Zhou, T. Zhu, T. Gao, P. Yan and H. Li, *ACS Appl. Mater. Interfaces*, 2020, **12**, 15338–15347.
55 X.-F. Duan, H.-H. Ji, L.-P. Zhou, S.-J. Hu, J.-J. Fu, P.-F. Duan, X.-Q. Guo and Q.-F. Sun, *CCS Chem.*, 2025, DOI: **10.31635/ccschem.024.202405005**, Just Accepted.